Mechanics of Time-Dependent Materials (2023) 28:2069–2083
https://doi.org/10.1007/s11043-023-09604-0

RESEARCH

Evaluating the viscoelastic shear properties of clear wood via off-axis compression testing and digital-image correlation

Rhodel Bengtsson[1] · Louis Bergeron[2] · Reza Afshar[1] · Mahmoud Mousavi[1] · E. Kristofer Gamstedt[1]

Received: 16 February 2023 / Accepted: 2 May 2023 / Published online: 17 May 2023

Abstract

Highly anisotropic materials like wood and unidirectional polymer composite structures are sensitive to shear deformations, in particular close to fixed joints. Large wooden structures in buildings and, e.g. wind-turbine blades, are designed to last for decades, and hence are susceptible to unwanted creep deformations. For improved structural design, the shear-creep properties of the material are needed. These are rarely available in the literature, possibly because of technical difficulties to achieve a well-defined shear-stress state in test specimens. For cost-efficient testing, this goal of a pure stress state necessarily needs to be compromised. In the present study, we propose a simple test method based on uniaxial compression on wooden cubes, but is equally applicable for fibre composites. The viscoelastic shear properties of Norway spruce (Picea abies) under off-axis creep compression tests have been characterised in all three directions. The tests are performed in a controlled climate chamber and the creep strains are captured using digital-image correlation.

Keywords Viscoelasticity · Experiment · Shear creep · Wood · Composites

✉ E.K. Gamstedt
kristofer.gamstedt@angstrom.uu.se

R. Bengtsson
rhodel.bengtsson@angstrom.uu.se

L. Bergeron
louis.bergeron@ens2m.org

R. Afshar
reza.afshar@angstrom.uu.se

M. Mousavi
mahmoud.mousavi@angstrom.uu.se

1 Division of Applied Mechanics, Department of Materials Science and Engineering, Uppsala University, Box 35, Uppsala, SE-75103, Sweden

2 Ecole Nationale Supérieure de Mécanique et des Microtechniques, 26, rue de l'Epitaphe, Besançon Cedex, 25030, France

1 Introduction

Since prehistoric times, wood has been used as a building material due to its unrivalled properties and abundance. It is still considered as an excellent building material due to its high stiffness to weight ratio, flexibility and damage tolerance. Recently, wood is seeing a renaissance as a renewable and sustainable building material. For a more widespread use of wood materials in structures, it is necessary to characterise their structural properties more thoroughly.

Large wooden structures in buildings and composites, in e.g. wind-turbine blades, are designed to last for decades, and hence are susceptible to unwanted creep deformations [Heinrichs and Naughton (2014), Holzer et al. (1989)]. For improved structural design, the shear-creep properties of the material are needed.

Wood can be considered as an orthotropic material with three material directions: longitudinal (L), radial (R) and tangential (T) in a cylindrical coordinate system. There have been numerous research studies on the static and time-dependent behaviour of wood in the normal directions, i.e. the L, T and R directions [Vorobyev (2017), Ozyhar et al. (2013), Jiang et al. (2016), Afshar et al. (2020)]. An experimental method to find the normal-creep properties of wood using small cubic samples under compression has been used, see Afshar et al. (2020). However, despite the importance of knowing the full three-dimensional behaviour of materials, the time-dependent shear behaviour of wood in the different planes, i.e. LT, LR and RT, is rarely available in the literature.

Shear testing of materials often leads to challenges with experimental setup and test performance. In principle, it is inevitable that both normal and shear stresses exist in the material plane being tested. It is therefore very difficult to perform a pure shear-stress condition.

To the knowledge of the authors, there have only been two studies on the shear-creep behaviour of wood in a constant climate. In Schniewind and Barrett (1972), plate shear tests were made according to the ASTM Designation D 805-63 standard, which were extended into a creep test. The experiments were done with Douglas fir wood in a constant-climate room with 50% relative humidity (RH) and at 22 °C. The shear-creep compliances were later obtained by using the deflection in relation to the point loads on the plate samples. In Hayashi et al. (1993), an off-axis tensile test was extended into a creep test. Rectangular specimens with fibres oriented at a certain angle with respect to the applied load were subjected to a constant tensile load. The creep strains were obtained using strain gauges and post-processed to obtain the shear-creep compliance using well-known tensor-transformation laws. The experiments of Hayashi et al. (1993) were also performed in a constant climate, but at 25 °C and 30% RH.

Due to the scarcity of data on the time-dependent shear behaviour of wood, it is hard to cross-verify the results described above. Numerical works, such as those by Ormarsson et al. (2010) and Fortino et al. (2009), are limited in their verification of their viscoelastic model during shear, and have taken estimates of the shear-creep behaviour via various assumptions or simplifications. Without measured creep properties, there is a risk of imprecise predictions in numerical models. There is a clear need to add more experimental shear-creep data (in LR, LT and RT) for various wood species. A first step in this direction is to conceive a test method that can be used to acquire these data, and show how it works within a feasible time frame. In the present study, we propose a simple test setup based on uniaxial compression on wooden cubes. We use the same experimental setup used in Afshar et al. (2020), as shown in Fig. 1, in a constant-climate chamber to perform our shear-creep experiments. The setup uses dead-loads to apply a compression load on smaller samples. Similarly to the off-axis tests in Hayashi et al. (1993), the wooden cube samples have their material direction

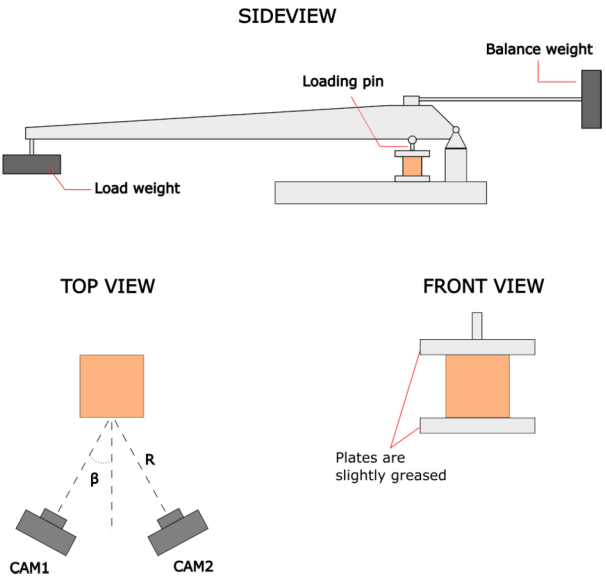

Fig. 1 Schematic illustration of the experimental setup of this study. The load from the weight to the left is transferred via the jointed loading pin then later to the upper plate to compress the sample. The purpose of the balance weight is to counteract the weight of the thick-beam setup. The positioning of the cameras are defined by $\beta = 15°$ and $R = 150$ mm. The plates that compress the sample are slightly greased to simulate rolling supports and avoid barrelling [Odgaard and Linde (1991), Narayanasamy et al. (1988)]

oriented at a given angle with respect to the applied compression load, allowing us to use transformation laws to determine the shear-creep compliance in different planes (RT, LR or LT). We use digital-image correlation (DIC) to determine the creep strains, from which the shear-creep compliance for the Norway Spruce samples are characterised in the RT, LR and LT planes. The approach is applicable not only to other wooden species, but also to composites that possess orthotropic behaviour.

2 Method

2.1 Experimental setup

The experiments were performed in a controlled climate with a relative humidity (RH) of $65 \pm 2\%$ and a temperature of 22 ± 1 °C. Three different sample types were prepared to capture the shear-creep behaviour in RT, LR and LT. Prior to testing, the samples had been conditioned with the same climate conditions for three months. The samples are of Norway spruce, which are locally sourced from Uppsala, Sweden. Five cubic samples of each type were cut and machined from clear wood of Norway Spruce. After conditioning, the density of the samples was 440 ± 32 kg/mm^3. The material directions of each specimen type were orientated in a similar manner to those shown in Fig. 2. The dimensions of the cubic samples were $15 \times 15 \times 15$ mm^3. A schematic showing how the LR sample were cut is shown in Fig. 3. As discussed by Walley and Rogers (2022) and Afshar (2022), small specimens usually mean a larger variability in behaviour. However, one advantage is that the curvatures of the annual rings are large in comparison to the specimen dimension. Due to this, the samples can be regarded as orthotropic in a Cartesian sense, rather than polar orthotropic. After considering this trade-off, Afshar et al. (2020) chose similar dimensions for their samples. The effects of polar orthotropic in uniaxial testing is further discussed in Shipsha and Berglund (2007).

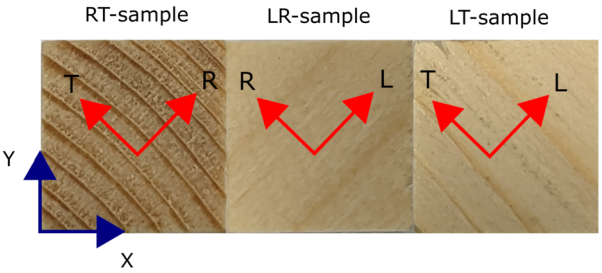

Fig. 2 Three types of samples were prepared. The samples are prepared in such a way that the plane of interest is rotated 45° around the global z-axis and from the global x-axis. The compression load is applied along the global y-axis

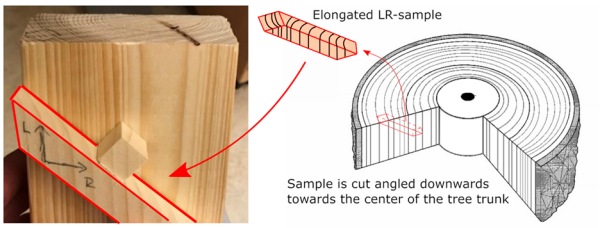

Fig. 3 For the LR samples, the elongated samples were cut angled downwards towards the centre of the trunk. These were later cut into cubes for the compression creep tests. The LT samples were prepared in a similar fashion, but were cut tangent to the annual rings instead

One sample at a time was inserted into the experimental setup shown in Fig. 1. The setup itself is contained inside a climate chamber with a constant temperature of 22 ± 1 °C and $65 \pm 2\%$ RH. Knowing the masses in the far ends of the lever, the compression load in Fig. 1 can be calculated from force and moment equilibrium around the support location. The applied compression load was chosen to be 5 MPa for LR and LT samples, and 1 MPa for the RT samples. The stresses were equal to roughly half of the measured shear strengths presented in Dahl and Malo (2009). Before applying the full load, the samples were pre-loaded with 2.5 MPa for the LR and LT samples, and 0.5 MPa for the RT samples. The main purpose of the pre-load is to smooth out the possible unevenness of the contact surfaces due to manufacturing of the samples. The samples were pre-loaded for 30 minutes, unloaded for two hours, thereafter the full load was applied for 24 hours. A pre-study was done to see if there was any unrecovered creep strains after unloading the samples from the pre-load. It was shown that there was in fact creep strains that remained after two hours and amounted to about 5–8% of the measured strains during the pre-load duration. When comparing these unrecovered strains to the strains measured in the creep test itself, they amounted to roughly 3–4% (due to the full load being double the pre-load).

Since the main purpose of this first study is to develop a practical test method, we have limited ourselves to this relatively short test period. This is similar to other creep investigations of wood materials, e.g. Ozyhar et al. (2013), Hayashi et al. (1993) and Jiang et al. (2016). For design purposes, much longer test times are obviously needed to reduce errors stemming from extrapolation.

2.2 Stereo DIC measurements

Stereo digital-image correlation (DIC) was chosen to measure the strain fields in our experiments. Stereo DIC, also known as 3D DIC, is a well-assessed non-contact full-field optical technique for measuring in-plane and out-of-plane displacement fields of a deforming object [Sutton et al. (2009), Cardenas-Garcia et al. (1995)]. A series of image pairs captured from two different angles of the object are used to locate and track, by means of triangulation, a given set of surface points during deformation, and calculate the displacement–strain field

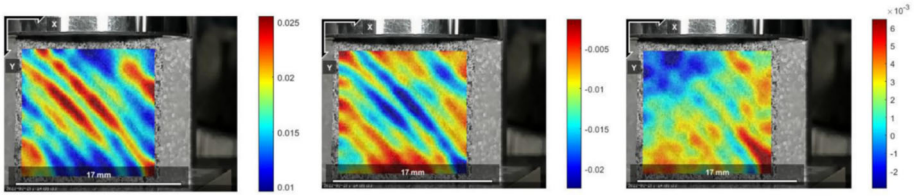

Fig. 4 Strain fields on one of the samples at the end of the creep test

of said surface. This method requires extensive camera calibration and determination of the relative position and orientation of the coordinate systems associated to the two cameras. Although the single-camera method (2D DIC) is far simpler to carry out, we opted for stereo DIC, since 2D DIC cannot capture the out-of-plane deformations, which were found to have a non-negligible influence on the determination of in-plane deformations in compression of wood cubes, especially in the LR and LT material directions. Such artifacts can be avoided by a stereo-camera approach [Jones and Iadicola (2018)].

In the present study, images of the surface of RT, LR or LT plane were continuously taken at 30-minute intervals over a 24-hour period with the cameras as seen in Fig. 1. The global strain fields of the surface were later calculated by the open-source stereo DIC algorithm, DuoDIC, by Solav and Silverstein (2022), which is an extension of the 2D DIC algorithm developed by Blaber et al. (2015). Distance and angles between samples and cameras are taken from the guidelines of Jones and Iadicola (2018).

Measurement errors are always of concern when determining small strains in DIC. In order to rule out uncertainty errors stemming from the measurement technique in the strain ranges during the creep tests, a pre-study was made with no applied load. These results are presented in the Appendix. In the present study, the order of magnitude of the measured strain for RT samples is 10^{-2}, and for LR and LT the strain is roughly 7×10^{-3}. The pre-study results shown in Fig. 11 in Appendix B show that the measured mean strain error is at most around 10% when compared to the measured strain magnitudes.

DIC is necessarily limited to the surface of the specimen. The strains in the interior of the specimen are therefore ignored in the calculation of the creep compliance. One may suggest using digital volume correlation to obtain the accurate description of the strain fields for the whole volume from X-ray computed tomography such as in Forsberg et al. (2010). This would require more costly equipment and handling significantly larger quantities of data. A simpler solution is to have thinner wood samples for which the plane-stress assumption is more appropriate, but would require further studies to avoid the buckling phenomena [Barile et al. (2019)].

The global y-coordinate system is parallel to the compression load, the x-coordinate is along the width of the cube specimen, and the z-coordinate is along the out-of-plane direction. Due to the inhomogeneity of wood, the strains were not homogeneous on the surface, as seen in Fig. 4. To simplify the post-processing of obtaining the material properties, the strain fields were averaged on the surface outlined by the region of interest in the DIC shown in Fig. 5. Henceforth in the text, strain values are referred to as the average values. The regions of interest were found by the largest square domain that presented a uniform average strain with limited edge effects.

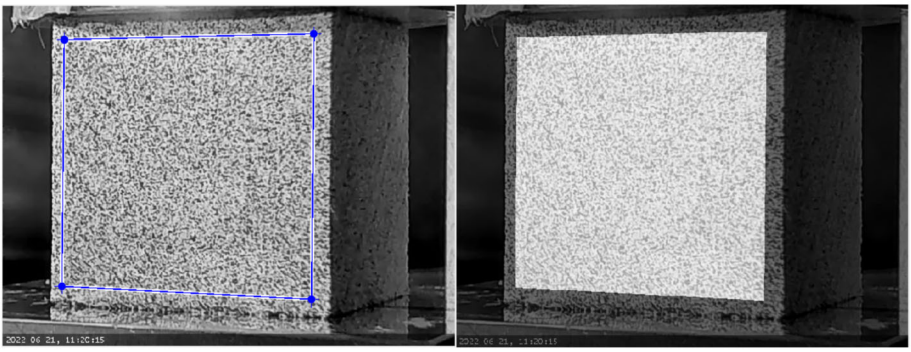

(a) (b)

Fig. 5 Region of interest of the DIC analysis: (a) Image of a speckled sample for DIC, and (b) of the region of interest highlighted. The averaging of the strain fields is taken over the highlighted surface

2.3 Material model

Since the applied force and sample dimensions are known, the applied compressive stress σ_y is readily determined and assumed to be homogeneous throughout the specimen. This assumption means that the effects of barrelling are neglected. The main cause of barrelling is the restraining friction between plates and specimen, as discussed by Odgaard and Linde (1991) and Narayanasamy et al. (1988).

The barrelling effect of compression of wooden cubes is discussed in Vorobyev et al. (2016), of which it amounted to at most a relative error of 1.5% in the Young's moduli in the normal directions.

The following equations were derived for the RT samples, but are easily reformulated for the LR and LT samples. Knowing the global stress and strains of a RT sample, the tensor fields according to the LRT-coordinate system are obtained by the following well-known transformation rules:

$$\varepsilon_{\mathrm{RT}} = (\varepsilon_x - \varepsilon_y)\sin\alpha\cos\alpha + \varepsilon_{xy}\cos 2\alpha \tag{1}$$

and

$$\sigma_{\mathrm{RT}} = (\sigma_x - \sigma_y)\sin\alpha\cos\alpha + \sigma_{xy}\cos 2\alpha. \tag{2}$$

It should be noted that the material axes in wood are typically designated LRT. For other orthotropic materials, other notations are used for the local coordinate systems, e.g. MD and CD for boards, and 123 for composites. Since the methods and expressions used in this work are pertinent not only to wood, the LRT coordinates can be readily be changed to any arbitrary notation for a given orthotropic material.

The relation between the evolution of creep strain and constant stress is described by the constitutive equation

$$\varepsilon(t) = J(t)\,\sigma_0. \tag{3}$$

The tensorial form of Eq. (3) is presented in the Appendix. In the present study, $\varepsilon(t)$ is the measured shear-creep strains $\varepsilon_{\mathrm{RT}}(t)$, $J(t)$ is the shear-creep compliance $J_{\mathrm{RT}}(t)$ and σ_0 is

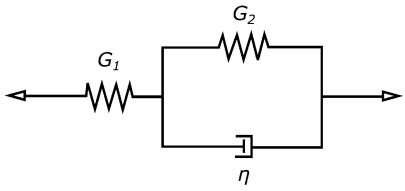

Fig. 6 Kelvin representation of the standard linear solid model (Tschoegl (2012))

equal to σ_{RT}. From the DIC analysis, discrete values of ε_x, ε_y and ε_{xy} at the sampling time $t = t_n$ are obtained and inputted into Eq. (1) to retrieve $\varepsilon_{\mathrm{RT}}(t_n)$. Having our only non-zero stress component as our constant applied compressive stress, σ_{y} allows us to retrieve our σ_{RT} via Eq. (2). For both cases above, α is carefully measured on the surface on the samples individually, but is roughly 45° in general.

From the obtained strain fields and the transformations in Eqs. (1) and (2), the shear-creep compliance at discrete values in time, $J_{\mathrm{RT}}(t = t_n)$, can be determined from Eq. (3). To define the continuous function $J_{\mathrm{RT}}(t)$, the discrete points $J_{\mathrm{RT}}(t = t_n)$ can be fitted to any given rheological model. In the present case, we chose the well-known linear viscoelastic-creep model known as the standard linear solid (SLS) model. The SLS model is one of the simplest viscoelastic models available to account for both elastic and diminishing time-dependent creep deformation. Both Afshar et al. (2020) and Huč and Svensson (2018) have used it to describe the creep behaviour of wood as observed in experiments. In the present study, the SLS model is a three-parameter model represented by a spring in series with a Voigt unit, the latter being a dashpot in parallel with another spring, schematically shown in Fig. 6. In Fig. 6, G_1 is the spring parameter of the first spring in the series, G_2 and η are the elastic- and viscous parameters describing the spring and dashpot inside the Voigt unit. The springs and dashpot can be regarded as elastic shear moduli and viscosity, respectively. The continuous creep compliance $J(t)$ in Eq. (3) can then be expressed as

$$\begin{aligned} J(t) &= \frac{1}{G_1} + \frac{1}{G_2}[1 - \exp(\frac{-tG_2}{\eta})] \\ &= J_g + J[1 - \exp(-t/\tau)], \end{aligned} \tag{4}$$

where $J_g = 1/G_1$, $J = 1/G_2$ and $\tau = \eta/G_2$. The response of this model to an instantaneous application of a constant stress is a sudden increase in strain followed by a delayed strain increase, until equilibrium is asymptotically reached when $t \to \infty$. This behaviour is solely dictated by the term inside the parenthesis in Eq. (4), which is equal to zero at $t = 0$ and goes towards unity when $t \to \infty$.

Hereafter, rather than using G_1, G_2 and η, the three parameters describing the SLS model will be J_g, J and τ. In this model, J_g may be regarded as the instantaneous compliance, and J is the delayed compliance.

With the present configuration of springs and dashpot in Fig. 6, the model cannot capture any permanent irreversible deformation after unloading (creep recovery), since the deformation fully reverts back to 0. Full recovery is usually not the case for wood, as seen by the creep tests by Taniguchi and Ando (2010). As a first step in shear-creep characterisation, irreversible deformations are ignored and only a three-parameter viscoelastic model is used without unloading, which is the case in many statically self-loaded structures. For more general cases considering permanent deformations, the readers are referred to Tschoegl (2012) and Ottosen and Ristinmaa (2005).

3 Results and discussion

In total, 15 creep tests were performed, of which five were for each sample type (RT, LR and LT). The samples were tested under constant climate at $65 \pm 2\%$ RH and 22 ± 1 °C. The creep-compliance curves for each sample type are presented in Figs. 7, 8 and 9, including an average curve in each diagram that represents the average behaviour of each sample type. The material parameters for each sample are presented in Tables 1, 2 and 3, using the same model as in Eq. (4).

The averaged creep curves for all three directions are compiled in Fig. 10. The LR compliance curve provided by Hayashi et al. (1993) is added for comparison. The rolling shear creep in the RT direction is presented in a separate graph, since the compliance is almost two orders of magnitude smaller than that in the stiffer LR and LT directions.

Since the shear-creep compliance in the RT plane and LT plane for Norway Spruce are, to the best knowledge of the authors, not available in the literature, it is not possible to compare the curves in Figs. 7 and 9 with any independent studies. However, the elastic-shear modulus determined from the instantaneous deformation when load is applied can be compared with literature values for Norway spruce. The shear-modulus values are presented in Table 4, and it can be seen that the measured values fall within the ranges found by other investigations.

As for the LR plane, however, one of the rare studies on shear creep [Hayashi et al. (1993)] can be compared with our new data (see Fig. 10). However, their LR curve was characterised at 30% RH and 25 °C, instead of at $65 \pm 2\%$ RH and 22 ± 1 °C in the present study. Our higher relative humidity implies a higher moisture content, and a more compliant behaviour, as is observed in Fig. 10. This amount of softening has also been shown by Fu et al. (2021) and Báder and Németh (2019), who measured an increase of compliance of 70–100% when the moisture content was increased from 5% to 10% in European beech.

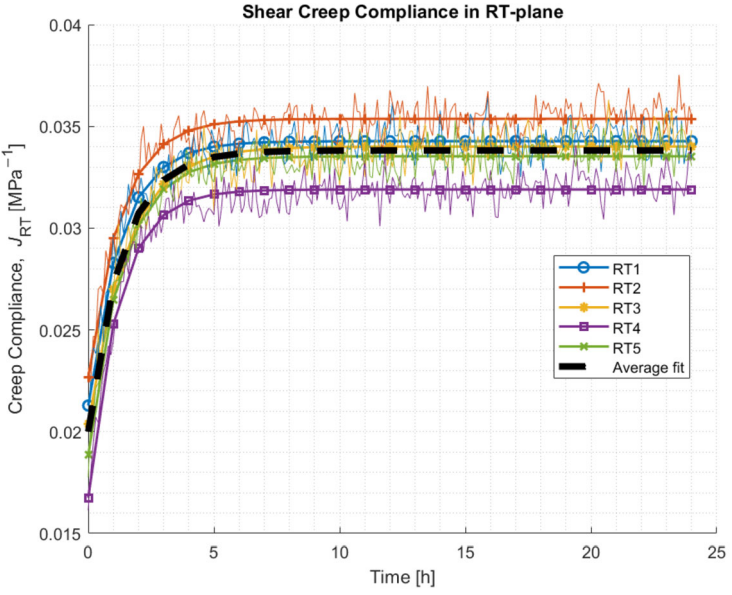

Fig. 7 Creep compliance for five different RT samples: Measurements, fitted SLS model for each sample and in average (dashed black line)

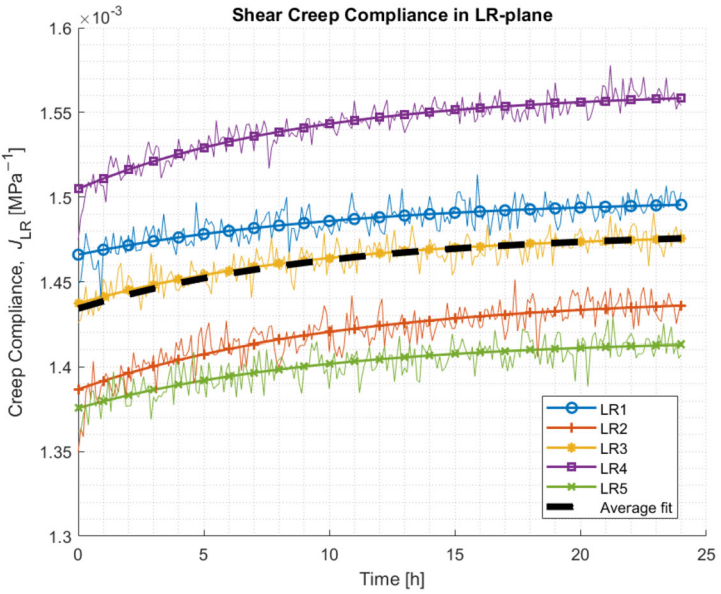

Fig. 8 Creep compliance from five different LR samples

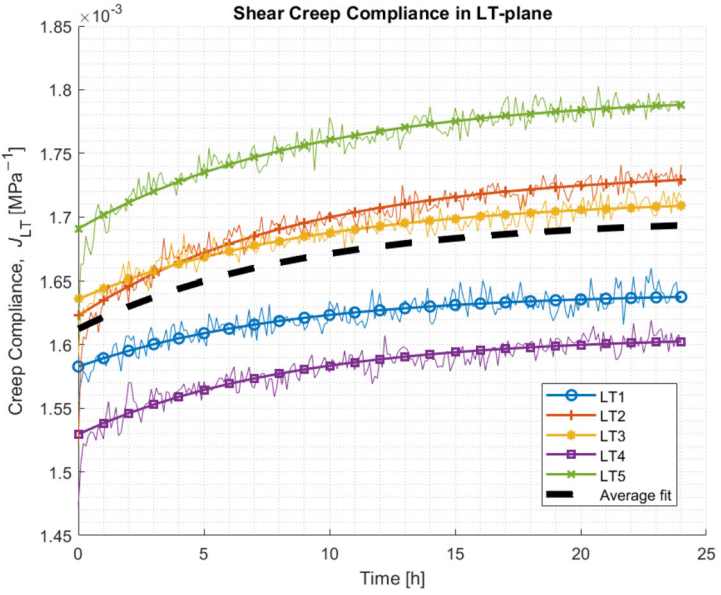

Fig. 9 Creep compliance from five different LT samples

Although the moisture content was not measured in the study by Hayashi et al. (1993) nor in the present study, it can be appraised by the relations of Simpson (1973). The moisture content from the sample of Hayashi et al. (1993) and the present study are then roughly

Table 1 Constitutive parameters for fitting the experimental RT data in Fig. 7 to the SLS model, including mean value and standard deviation

	J_g [MPa^{-1}]	J [MPa^{-1}]	τ [h]
RT1	0.0213	0.01298	1.290
RT2	0.0227	0.01268	1.299
RT3	0.0204	0.01362	1.506
RT4	0.0167	0.01514	1.205
RT5	0.0189	0.01467	1.365
μ	0.0199	0.01382	1.333
σ	0.0023	0.00650	0.123

μ – mean value. σ – standard deviation

Table 2 Model parameters for fitting LR data points in Fig. 8 including statistical measurements of the parameters

	J_g [MPa^{-1}]	J [MPa^{-1}]	τ [h]
LR1	1.466×10^{-3}	3.306×10^{-5}	10.87
LR2	1.388×10^{-3}	5.466×10^{-5}	10.41
LR3	1.436×10^{-3}	4.181×10^{-5}	9.49
LR4	1.505×10^{-3}	5.750×10^{-5}	9.17
LR5	1.375×10^{-3}	4.076×10^{-5}	9.78
μ	1.434×10^{-3}	4.556×10^{-5}	9.94
σ	5.413×10^{-5}	1.023×10^{-5}	0.69

μ – mean value. σ – standard deviation

Table 3 Model parameters for fitting LT data points in Fig. 9, including statistical measurements of the parameters

	J_g [MPa^{-1}]	J [MPa^{-1}]	τ [h]
LT1	1.5829×10^{-3}	5.7932×10^{-5}	8.34
LT2	1.6232×10^{-3}	1.1355×10^{-4}	8.94
LT3	1.6359×10^{-3}	7.8870×10^{-5}	9.41
LT4	1.5299×10^{-3}	7.7164×10^{-5}	8.45
LT5	1.6911×10^{-3}	1.0504×10^{-4}	9.24
μ	1.612×10^{-3}	8.6523×10^{-5}	8.87
σ	6.206×10^{-5}	2.2571×10^{-5}	0.47

μ – mean value. σ – standard deviation

Table 4 Shear-modulus values obtained at $t = 0$ for all samples. Literature value ranges for Norway Spruce are also presented, although quantified using different test methods under climate conditions (Keunecke et al. (2007), Ehrhart and Brandner (2018), Karakoç et al. (2013), Dahl and Malo (2009), Sretenovic et al. (2004), Persson (2000))

	Sample 1	Sample 2	Sample 3	Sample 4	Sample 5	μ	Lit. values
G_{RT} [MPa]	49.46	43.26	52.24	61.94	56.28	52.0	20.0–90.0
G_{LR} [MPa]	690.4	741.0	701.3	678.1	734.1	709.0	600.0–800.0
G_{LT} [MPa]	791.13	643.5	657.4	628.7	619.9	645.6	600.0–750.0

μ – mean value.

estimated to be 6% and 12%, respectively, which compare well with the aforementioned studies.

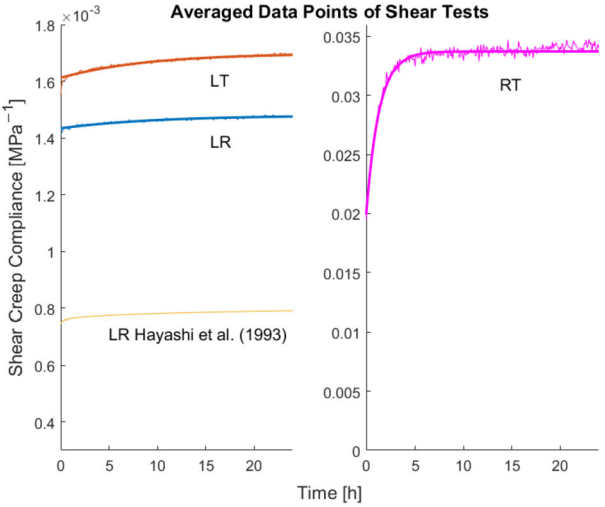

Fig. 10 Averaged compliance data points from shear-creep tests for LT, LT and RT, with their respective fits to the SLS model. In the left plot, the LR shear-creep curve from Hayashi et al. (1993) is presented for comparison

As mentioned previously, the samples had to be pre-loaded to further flatten and even out the surfaces from the machining process of the samples. There is a slight discrepancy of not considering the full history of the samples when retrieving the parameters, as unrecovered strains were observed after the pre-load. Another issue is the SLS model itself since it cannot mathematically consider unrecovered creep strains due to its spring/dashpot configuration, thus an entirely different model should be used to capture this behaviour.

This study has been focused on shear creep only, motivated by a striking lack of data in the literature and usefulness of presenting a straightforward and relatively easy method that could be implemented in most mechanical testing laboratories. Although not well reported, there are more data on normal creep along the main material axes for wood than for shear creep [e.g. Vorobyev (2017), Ozyhar et al. (2013), Jiang et al. (2016), Afshar et al. (2020)]. Due to time constraints, the normal creep was not characterised here, even though both shear- and normal-creep data are needed to formulate the full creep compliance matrix for finite-element implementation to predict creep deformation in a component made of orthotropic wood. Bengtsson et al. (2022) presented how to implement a full 3D viscoelastic model in a finite-element environment using material parameters in the normal directions extrapolated from experimental data Ozyhar et al. (2013). Due to the lack of any shear-creep data, the model in question was assumed to behave elastically in pure shear. With this new method at hand, shear-creep tests can be carried out relatively easily. The resulting data can then be used as input to allow time-dependent shear components in the finite-element model.

The 24-hour duration used in the present study was chosen for practical reasons to produce more data in a shorter period of time. Thus, the resulting material parameters may not be reliable for use far beyond 24 hours. The readers are referred to the works by Hunt (2004) on how to extrapolate long-time viscoelastic creep behaviour from short-time data, specifically for wood. Regardless, there is no reason to believe that the creep experiments in this study cannot be extended to a longer duration and retrieve material parameters for more realistic time frames in engineering design. For instance, Laufenberg (1999) conducted creep tests on wood up to 8 weeks. This duration was motivated via a corresponding typical snow-loaded season.

4 Concluding remarks

We have presented a viable creep setup to obtain the shear-creep compliance of wooden samples for the RT, LR and LT planes in uniaxial compression. No intricate test jigs or equipment are required for this method, as the setup only relies on the orientation of the material directions inside the wooden cube and testing in compression. Although the method was used for Norway Spruce, it is equally applicable for other types of wood species as well as other composite materials that possess orthotropic behaviour. The simplicity of the method is considered to compensate for some amount of inevitable non-uniformity in stress and deformation fields that could be reduced in more complicated setups for tensile loading of slender specimens.

The material parameters of the shear-creep behaviour have been presented in Tables 1 to 3. These data could in principle be used in finite-element models. For rheological models other than the SLS model used here, one would have to re-fit the data with the particular material model. Indeed, the creep behaviour in the normal direction of Norway Spruce is not within the scope of this study, and thus the authors refer to the works of Vorobyev (2017), Ozyhar et al. (2013), Jiang et al. (2016), Afshar et al. (2020) on how to extract the creep data in the normal direction, including the Poisson behaviour during creep. After having the full 3D viscoelastic representation for a particular type of wood, it would be possible to simulate the time-dependent behaviour of wood in a constant climate.

The main accomplishment here is the creep-behaviour characterisation in all shear directions shown in Figs. 7 to 9 by means of a straightforward test method. A next step would be to verify these with an independent method. The only verification made so far is that the elastic-shear moduli in Table 4 were found to be well within the range of corresponding literature values.

Appendix A: Equation in tensorial form

The equations used in the present study may be presented in tensorial form. The creep strain can then be determined given a constant stress state

$$\varepsilon_{ij}(t) = J_{ijkl}(t)\sigma_{kl}. \tag{A.1}$$

Following the locally Cartesian LRT coordinate system and considering the shear-creep strain, ε_{RT}, Eq. (A.1) is expressed as

$$\begin{aligned}\varepsilon_{\mathrm{RT}}(t) &= J_{\mathrm{RT}kl}(t)\sigma_{kl}\\ &= J_{\mathrm{RTRR}}(t)\sigma_{\mathrm{RR}} + 2J_{\mathrm{RTRT}}(t)\sigma_{\mathrm{RT}} + J_{\mathrm{RTTT}}(t)\sigma_{\mathrm{TT}}.\end{aligned} \tag{A.2}$$

Assuming orthotropic symmetry, the fourth-order creep compliance tensor, J_{ijkl} may be presented in matrix form using Voigt notation such as

$$J = \begin{bmatrix} J_{11} & J_{12} & J_{13} & 0 & 0 & 0\\ & J_{22} & J_{23} & 0 & 0 & 0\\ & & J_{33} & 0 & 0 & 0\\ & \text{Sym.} & & J_{44} & 0 & 0\\ & & & & J_{55} & 0\\ & & & & & J_{66} \end{bmatrix}, \tag{A.3}$$

with replacements $LL \rightarrow 1$, $RR \rightarrow 2$, $TT \rightarrow 3$, $LR \rightarrow 4$, $LT \rightarrow 5$, $RT \rightarrow 6$. Due to the zeros in Eq. (A.3), the shear strain $\varepsilon_{\mathrm{RT}}(t)$ in Eq. (A.2) is further simplified to

$$\begin{aligned} \varepsilon_{\mathrm{RT}}(t) &= J_{\mathrm{RTRR}}(t)\sigma_{\mathrm{RR}} + 2J_{\mathrm{RTRT}}(t)\sigma_{\mathrm{RT}} + J_{\mathrm{RTTT}}(t)\sigma_{\mathrm{TT}} \\ &= 2J_{\mathrm{RTRT}}(t)\sigma_{\mathrm{RT}} \\ &= J_{66}\sigma_{\mathrm{RT}} \\ &= J_{\mathrm{RT}}\sigma_{\mathrm{RT}}. \end{aligned} \quad . \tag{A.4}$$

For general anisotropy, e.g. $J_{66} \neq 0$, $J_{62} \neq 0$, more experiments are required to define the creep compliance. The LRT coordinate system is the preferred notation for orthotropic wood. These symbols can readily be exchanged for different notations pertinent to other orthotropic materials, e.g. fiber-reinforced plastics.

Appendix B: Measurement verification

A pre-study was carried out to quantify the systematic error caused by the measurement equipment in unloaded conditions. An RT sample was placed in the setup with no applied load for 24 hours. No load should imply no strain, and any measured strains from the DIC were considered as measurement errors. The results are presented in Fig. 11. The results showed that the measured error strains were roughly 0.5×10^{-4}, which is small compared to the strains measured during the creep test.

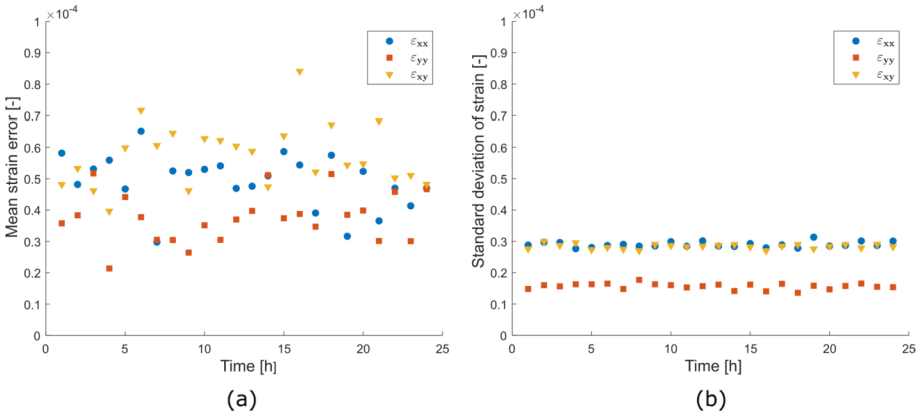

Fig. 11 Measured strains in a sample with no applied load. Any non-zero strains represent measurement errors shown in (a). The standard deviation represents the deviation from the average strain field at any given time, t_n, shown in (b). The scatter plots represent (a) the precision and (b) the accuracy of the experimental setup

Author contributions RB and LB performed the experiments with help from RA. RB wrote the main manuscript text. All authors interpreted the results and reviewed the manuscript. EKG conceived the idea and coordinated the project.

Funding Open access funding provided by Uppsala University. RB has been funded by the Swedish Research Council, grant 2016-04534.

Declarations

Competing interests The authors declare no competing interests.

References

Afshar, R.: Characterisation of mechanical properties of wood: size effect. In: Theoretical Analyses, Computations, and Experiments of Multiscale Materials, pp. 659–669. Springer, Berlin (2022). https://doi.org/10.1007/978-3-031-04548-6_30

Afshar, R., Cheylan, M., Almkvist, G., et al.: Creep in oak material from the vasa ship: verification of linear viscoelasticity and identification of stress thresholds. Eur. J. Wood Prod. **78**(6), 1095–1103 (2020). https://doi.org/10.1007/s00107-020-01566-1

Báder, M., Németh, R.: Moisture-dependent mechanical properties of longitudinally compressed wood. Eur. J. Wood Prod. **77**(6), 1009–1019 (2019)

Barile, C., Casavola, C., Pappalettera, G.: Digital image correlation comparison of damaged and undamaged aeronautical cfrps during compression tests. Materials **12**(2), 249 (2019). https://doi.org/10.3390/ma12020249

Bengtsson, R., Afshar, R., Gamstedt, E.K.: An applicable orthotropic creep model for wood materials and composites. Wood Sci. Technol. **56**(6), 1585–1604 (2022). https://doi.org/10.1007/s00226-022-01421-x

Blaber, J., Adair, B., Antoniou, A.: Ncorr: open-source 2d digital image correlation Matlab software. Exp. Mech. **55**(6), 1105–1122 (2015). https://doi.org/10.1007/s11340-015-0009-1

Cardenas-Garcia, J., Yao, H., Zheng, S.: 3d reconstruction of objects using stereo imaging. Opt. Lasers Eng. **22**(3), 193–213 (1995). https://doi.org/10.1016/0143-8166(94)00046-D

Dahl, K.B., Malo, K.: Linear shear properties of spruce softwood. Wood Sci. Technol. **43**(5), 499–525 (2009). https://doi.org/10.1007/s00226-009-0246-5

Ehrhart, T., Brandner, R.: Rolling shear: test configurations and properties of some European soft-and hardwood species. Eng. Struct. **172**, 554–572 (2018). https://doi.org/10.1016/j.engstruct.2018.05.118

Forsberg, F., Sjödahl, M., Mooser, R., et al.: Full three-dimensional strain measurements on wood exposed to three-point bending: analysis by use of digital volume correlation applied to synchrotron radiation micro-computed tomography image data. Strain **46**(1), 47–60 (2010). https://doi.org/10.1111/j.1475-1305.2009.00687.x

Fortino, S., Mirianon, F., Toratti, T.: A 3d moisture-stress fem analysis for time dependent problems in timber structures. Mech. Time-Depend. Mater. **13**(4), 333–356 (2009). https://doi.org/10.1007/s11043-009-9103-z

Fu, W.L., Guan, H.Y., Kei, S.: Effects of moisture content and grain direction on the elastic properties of beech wood based on experiment and finite element method. Forests **12**(5), 610 (2021)

Hayashi, K., Felix, B., Le Govic, C.: Wood viscoelastic compliance determination with special attention to measurement problems. Mater. Struct. **26**(6), 370–376 (1993)

Heinrichs, T.D., Naughton, B.T.: (2014). Radar friendly blades. Tech. Rep., Sandia National Lab. (SNL-NM), Albuquerque, NM (United States)

Holzer, S.M., Loferski, J.R., Dillard, D.A.: A review of creep in wood: concepts relevant to develop long-term behavior predictions for wood structures. Wood Fiber Sci. 376–392 (1989)

Huč, S., Svensson, S.: Coupled two-dimensional modeling of viscoelastic creep of wood. Wood Sci. Technol. **52**(1), 29–43 (2018). https://doi.org/10.1007/s00226-017-0944-3

Hunt, D.: The prediction of long-time viscoelastic creep from short-time data. Wood Sci. Technol. **38**(7), 479–492 (2004). https://doi.org/10.1007/s00226-004-0244-6

Jiang, J., Valentine, B.E., Lu, J., et al.: Time dependence of the orthotropic compression young's moduli and Poisson's ratios of Chinese fir wood. Holzforschung **70**(11), 1093–1101 (2016). https://doi.org/10.1515/hf-2016-0001

Jones, E., Iadicola, M.: A good practices guide for digital image correlation. A good practices guide for digital image correlation. International Digital Image Correlation Society (2018). https://doi.org/10.32720/idics/gpg.ed1

Karakoç, A., Tukiainen, P., Freund, J., et al.: Experiments on the effective compliance in the radial–tangential plane of Norway spruce. Compos. Struct. **102**, 287–293 (2013). https://doi.org/10.1016/j.compstruct.2013.03.013

Keunecke, D., Sonderegger, W., Pereteanu, K., et al.: Determination of young's and shear moduli of common yew and Norway spruce by means of ultrasonic waves. Wood Sci. Technol. **41**(4), 309–327 (2007). https://doi.org/10.1007/s00226-006-0107-4

Laufenberg, T.: Creep and creep-rupture behavior of wood-based structural panels, vol. 574. US Department of Agriculture, Forest Service, Forest Products Laboratory (1999)

Narayanasamy, R., Murthy, R., Viswanatham, K., et al.: Prediction of the barreling of solid cylinders under uniaxial compressive load. J. Mech. Work. Technol. **16**(1), 21–30 (1988)

Odgaard, A., Linde, F.: The underestimation of young's modulus in compressive testing of cancellous bone specimens. J. Biomech. **24**(8), 691–698 (1991)

Ormarsson, S., Dahlblom, O., Johansson, M.: Numerical study of how creep and progressive stiffening affect the growth stress formation in trees. Trees **24**(1), 105–115 (2010). https://doi.org/10.1007/s00468-009-0383-3

Ottosen, N.S., Ristinmaa, M.: The Mechanics of Constitutive Modeling. Elsevier, Amsterdam (2005)

Ozyhar, T., Hering, S., Niemz, P.: Viscoelastic characterization of wood: time dependence of the orthotropic compliance in tension and compression. J. Rheol. **57**(2), 699–717 (2013). https://doi.org/10.1122/1.4790170

Persson, K.: Micromechanical modelling of wood and fibre properties. Lund University, Department of Mechanics and Materials Lund (2000)

Schniewind, A.P., Barrett, J.: Wood as a linear orthotropic viscoelastic material. Wood Sci. Technol. **6**(1), 43–57 (1972)

Shipsha, A., Berglund, L.A.: Shear coupling effects on stress and strain distributions in wood subjected to transverse compression. Compos. Sci. Technol. **67**(7–8), 1362–1369 (2007). https://doi.org/10.1016/j.compscitech.2006.09.013

Simpson, W.T.: Predicting equilibrium moisture content of wood by mathematical models. Wood and fiber science, 41–49 (1973)

Solav, D., Silverstein, A.: Duodic: 3d digital image correlation in Matlab. J. Open Sour. Softw. **7**(74), 4279 (2022). https://doi.org/10.21105/joss.04279

Sretenovic, A., Müller, U., Gindl, W., et al.: New shear assay for the simultaneous determination of shear strength and shear modulus in solid wood: finite element modeling and experimental results. Wood and fiber science, 302–310 (2004)

Sutton, M.A., Orteu, J.J., Schreier, H.: Image Correlation for Shape, Motion and Deformation Measurements: Basic Concepts, Theory and Applications. Springer, Berlin (2009)

Taniguchi, Y., Ando, K.: Time dependence of Poisson's effect in wood I: the lateral strain behavior. J. Wood Sci. **56**(2), 100–106 (2010). https://doi.org/10.1007/s10086-009-1070-0

Tschoegl, N.W.: The Phenomenological Theory of Linear Viscoelastic Behavior: An Introduction. Springer, Berlin (2012)

Vorobyev, A.: Static and time-dependent mechanical behaviour of preserved archaeological wood: Case studies of the seventeenth century warship vasa. PhD thesis, Acta Universitatis Upsaliensis (2017)

Vorobyev, A., Bjurhager, I., van Dijk, N.P., et al.: Effects of barrelling during axial compressive tests of cubic samples with isotropic, transversely isotropic and orthotropic elastic properties. Compos. Sci. Technol. **137**, 1–8 (2016). https://doi.org/10.1016/j.compscitech.2016.10.015

Walley, S.M., Rogers, S.J.: Is wood a material? Taking the size effect seriously. Materials **15**(15), 5403 (2022). https://doi.org/10.3390/ma15155403